

Synthesis, 3D-QSAR, and docking studies of 1-phenyl-1*H*-1,2,3-triazoles as selective antagonists for β_3 over $\alpha_1\beta_2\gamma_2$ GABA receptors

Mohammad Sayed Alam,^a Jia Huang,^a Fumiyo Ozoe,^a
Fumio Matsumura^b and Yoshihisa Ozoe^{a,*}

^aDepartment of Life Science and Biotechnology, Faculty of Life and Environmental Science, Shimane University, Matsue, Shimane 690-8504, Japan

^bDepartment of Environmental Toxicology and the Center for Environmental Health Sciences, University of California, Davis, CA 95616, USA

Received 31 March 2007; revised 13 May 2007; accepted 15 May 2007

Available online 18 May 2007

Abstract—A series of 16 1-phenyl-1*H*-1,2,3-triazoles with substituents at both the 4- and 5-positions of the triazole ring were synthesized, and a total of 49 compounds, including previously reported 4- or 5-monosubstituted analogues, were examined for their ability to inhibit the specific binding of [³H]4'-ethynyl-4-*n*-propylbicycloorthobenzoate (EBOB), a non-competitive antagonist, to human homo-oligomeric β_3 and hetero-oligomeric $\alpha_1\beta_2\gamma_2$ γ -aminobutyric acid (GABA) receptors. Among all tested compounds, the 4-*n*-propyl-5-chloromethyl analogue of 1-(2,6-dichloro-4-trifluoromethylphenyl)-1*H*-1,2,3-triazole showed the highest level of affinity for both β_3 and $\alpha_1\beta_2\gamma_2$ receptors, with *K*_i values of 659 pM and 266 nM, respectively. Most of the tested compounds showed selectivity for β_3 over $\alpha_1\beta_2\gamma_2$ receptors. Among all 1-phenyl-1*H*-1,2,3-triazoles, the 4-*n*-propyl-5-ethyl analogue exhibited the highest (>1133-fold) selectivity, followed by the 4-*n*-propyl-5-methyl analogue of 1-(2,6-dibromo-4-trifluoromethylphenyl)-1*H*-1,2,3-triazole with a >671-fold selectivity. The 2,6-dichloro plus 4-trifluoromethyl substitution pattern on the benzene ring was found to be important for the high affinity for both β_3 and $\alpha_1\beta_2\gamma_2$ receptors. Comparative molecular field analysis (CoMFA) and comparative molecular similarity indices analysis (CoMSIA) provided similar contour maps, revealing that an electronegative substituent at the 4-position of the benzene ring, a compact, hydrophobic substituent at the 4-position of the triazole ring, and a small, electronegative substituent at the 5-position of the triazole ring play significant roles for the high potency in β_3 receptors. Molecular docking studies suggested that the putative binding sites for 1-phenyl-1*H*-1,2,3-triazole antagonists are located in the channel-lining 2'-6' region of the second transmembrane segment of β_3 and $\alpha_1\beta_2\gamma_2$ receptors. A difference in the hydrophobic environment at the 2' position might underlie the selectivity of 1-phenyl-1*H*-1,2,3-triazoles for β_3 over $\alpha_1\beta_2\gamma_2$ receptors. The compounds that had high affinity for β_3 receptors with homology to insect GABA receptors showed insecticidal activity against houseflies with LD₅₀ values in the pmol/fly range. The information obtained in the present study should prove helpful for the discovery of selective insect control chemicals.

© 2007 Elsevier Ltd. All rights reserved.

1. Introduction

γ -Aminobutyric acid (GABA) is the major inhibitory neurotransmitter ubiquitously distributed in the central nervous system of both vertebrates and invertebrates. GABA exerts its inhibitory effect through two types of membrane receptors, the ionotropic and the G pro-

tein-coupled metabotropic receptors, to regulate the function of the nervous system.¹ The ionotropic GABA receptors belong to a family of ligand-gated ion channels that include nicotinic acetylcholine receptors, glycine receptors, and serotonin type 3 receptors.² The mammalian ionotropic GABA receptors are heteropentamers composed of five subunits forming a central chloride ion channel. GABA binds to the agonist binding site of GABA receptors in the cell membrane and influences the opening of the built-in channels to increase the chloride ion influx into the cell, which results in suppression of nerve excitation.³ To date, 19 subunits (α_1 – α_6 , β_1 – β_3 , γ_1 – γ_3 , ρ_1 – ρ_3 , δ , ϵ , π , and θ) of GABA receptors

Keywords: GABA receptor; Antagonist; 3D-QSAR; Homology model; Phenyltriazoles.

* Corresponding author. Fax: +81 852 32 6092; e-mail: ozoe-y@life.shimane-u.ac.jp

have been identified in the nervous system, and have been classified according to their sequence identity.^{4,5} Although a number of different subunit compositions would have the potential to form the pentamers, only a limited number of combinations have been identified. The $\alpha 1\beta 2\gamma 2$ subunit composition is the most abundant, accounting for about 43% of GABA type A (GABA_A) receptors in the rat brain.⁶ Insect ionotropic GABA receptors are structurally similar to mammalian GABA_A receptors, although the two have different pharmacologies. Insect GABA receptors are not only localized in the central nervous system but also in the peripheral nervous system⁷; therefore, anti-GABAergic insecticides are thought to easily access these peripheral GABA receptors and thereby exert their insecticidal effects. At present, three different types of ionotropic GABA receptor subunits have been cloned from several different insect species; that is, RDL (a subunit encoded by the *Rdl* (resistant to dieldrin) gene), LCCH3 (ligand-gated chloride channel 3), and GRD (the GABA_A and glycine receptor-like subunit of *Drosophila*). RDL, which was first isolated from a naturally occurring dieldrin-resistant strain of *Drosophila melanogaster*,^{8,9} is capable of forming a chloride channel.

In order to pharmacologically characterize ionotropic GABA receptors, a number of non-competitive antagonists such as picrotoxinin and 4'-ethynyl-4-*n*-propyl-bicycloorthobenzoate (EBOB) (Fig. 1) have been utilized as probes, and a number of structurally diverse non-competitive antagonists have also been discovered to date.¹⁰ The binding site for the non-competitive antagonists is thought to be located within the channel pore, where they bind to stabilize the channel in a closed form and exert toxic effects. Fipronil (Fig. 1) is an effective, commercially available insecticide that acts at insect ionotropic GABA receptors as well as inhibitory glutamate receptors (glutamate-gated chloride channels).¹¹ Fipronil reduced GABA-induced currents in *Drosophila* RDL homo-oligomers stably expressed in a *Drosophila* S2 cell line¹² and in native GABA receptors of cockroach neurons.¹³ Fipronil also potently competes for the EBOB binding site in both native and recombinant GABA receptors.^{14–17} The selectivity of fipronil for insect versus mammalian GABA receptors might be due to the difference in their subunit compositions,¹⁶ which indicates that insect receptors differ significantly from their mammalian counterparts with respect to the structure of the non-competitive antagonist binding site. In a previous study, we reported that diverse classes of phenyl heterocyclic compounds also potently and selectively inhibit [³H]EBOB binding to insect GABA receptors.¹⁸

Recently, we have also reported the synthesis and structure–activity relationships of 4- or 5-substituted 1-phenyl-1*H*-1,2,3-triazoles (Fig. 1) as non-competitive antagonists that showed significant insecticidal action.¹⁹ In the present study, we further synthesized a new series of 1-phenyl-1*H*-1,2,3-triazoles with substituents at both the 4- and 5-positions of the triazole ring to study the molecular mechanisms of the interaction of phenyl heterocyclic compounds with GABA receptors. The affinities of 1-phenyl-1*H*-1,2,3-triazoles, including the newly and the previously synthesized series of analogues, for recombinant human $\beta 3$ and $\alpha 1\beta 2\gamma 2$ GABA receptors were determined by a competition assay using [³H]EBOB as a probe. The human $\beta 3$ receptor was used here as an insect GABA receptor model, since human $\beta 3$ and insect RDL GABA receptors were shown to have homologous amino acid sequences in the putative non-competitive antagonist binding site and similar pharmacological properties,^{15,17,19} and it should also be noted that such a homo-oligomeric $\beta 3$ ion channel has not been identified in the mammalian brain.²⁰ In the present study, we also performed three-dimensional quantitative structure–activity relationship (3D-QSAR) analysis to predict favorable and unfavorable moieties of 1-phenyl-1*H*-1,2,3-triazoles for high potency. Finally, we modeled docking of 1-phenyl-1*H*-1,2,3-triazoles to GABA receptors to predict the mechanisms of their receptor selectivity. Here we report the results of these efforts.

2. Results and discussion

2.1. Synthesis of 4,5-disubstituted 1-(substituted phenyl)-1*H*-1,2,3-triazoles

In the present study, a series of 16 4,5-disubstituted 1-(substituted phenyl)-1*H*-1,2,3-triazoles (Table 1) were synthesized by the 1,3-dipolar cycloaddition between a phenyl azide and an appropriate unsymmetrical alkyne, which gave a mixture of two regioisomers with substituents exchanged at the 4- and 5-positions (Scheme 1). The regioisomers were separated by silica gel column chromatography. Among the disubstituted phenyltriazoles containing alkyl groups at both the 4- and 5-positions of the triazole ring, the regioisomers with a long alkyl group at the 4-position were usually obtained in 1.3- to 1.6-fold higher yields than their corresponding isomers. The structures of the regioisomers of disubstituted 1-phenyl-1*H*-1,2,3-triazoles were determined on the basis of their ¹H NMR, mass spectrum, and elemental analysis data as well as on the data from our previous study.¹⁹ Compounds **15** and **16** were synthesized from

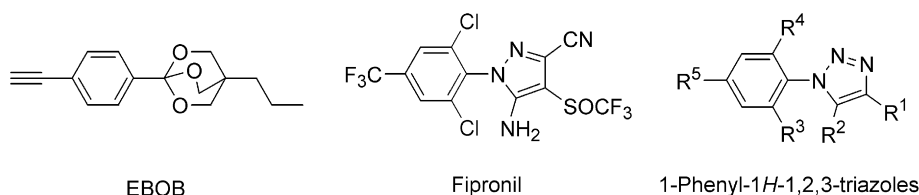
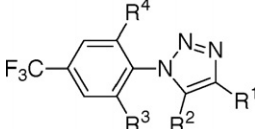


Figure 1. Structures of EBOB, fipronil, and 1-phenyl-1*H*-1,2,3-triazoles.

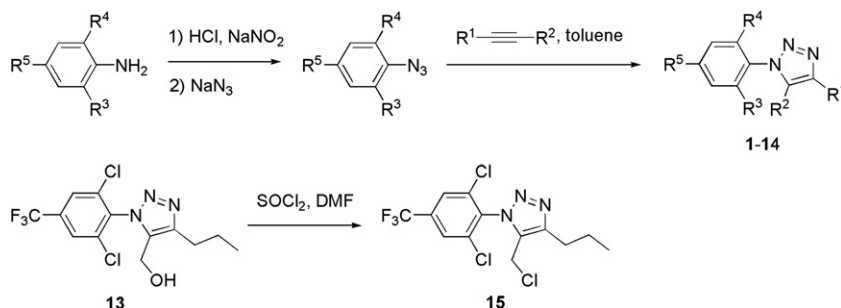
Table 1. Potencies of 4,5-disubstituted 1-(2,6-disubstituted 4-trifluoromethylphenyl)-1*H*-1,2,3-triazoles in inhibiting [³H]EBOB binding to $\beta 3$ and $\alpha 1\beta 2\gamma 2$ GABA receptors


Compound	R ¹	R ²	R ³ /R ⁴	K _i value		RS ^a
				$\beta 3$ (nM)	$\alpha 1\beta 2\gamma 2$ (μ M)	
1	Et	Me	Cl	7.08 (4.18–11.60 ^b)	1.06 (0.67–1.77 ^b)	150
2	Me	Et	Cl	70.1 (44.6–110.1 ^b)	>9.15	>131
3	Et	Et	Cl	4.27 (2.50–7.00 ^b)	0.959 (0.619–1.564 ^b)	225
4	<i>n</i> -Pr	Me	Cl	1.94 (1.17–3.08 ^b)	0.322 (0.187–0.558 ^b)	166
5	Me	<i>n</i> -Pr	Cl	539 (378–779 ^b)	>9.15	>17.0
6	<i>n</i> -Pr	Me	Br	13.6 (7.3–23.6 ^b)	>9.15	>673
10	<i>n</i> -Pr	Et	Cl	8.07 (5.19–12.25 ^b)	>9.15	>1130
11	Et	<i>n</i> -Pr	Cl	47.2 (31.3–70.4 ^b)	>9.15	>194
12	<i>n</i> -Pr	<i>n</i> -Pr	Cl	128 (78–208 ^b)	>9.15	>71.5
13	<i>n</i> -Pr	CH ₂ OH	Cl	2.53 (1.49–4.17 ^b)	0.387 (0.208–0.778 ^b)	153
14	CH ₂ OH	<i>n</i> -Pr	Cl	3450 (1980–7780 ^b)	>9.15	>2.65
15	<i>n</i> -Pr	CH ₂ Cl	Cl	0.659 (0.242–1.667 ^b)	0.266 (0.175–0.412 ^b)	403
16	CH ₂ Cl	<i>n</i> -Pr	Cl	66.7 (34.2–125.0 ^b)	>9.15	>137

Compounds with a K_i value of >8.00 μ M for $\beta 3$ receptors and a K_i value of >9.00 μ M for $\alpha 1\beta 2\gamma 2$ receptors: **7** (R¹ = Me, R² = *n*-Pr, R³/R⁴ = Br), **8** (R¹ = *n*-Pr, R² = Me, R³/R⁴ = H), and **9** (R¹ = Me, R² = *n*-Pr, R³/R⁴ = H).

^a Selectivity for $\beta 3$ versus $\alpha 1\beta 2\gamma 2$ receptors ($K_i^{\alpha 1\beta 2\gamma 2}/K_i^{\beta 3}$).

^b 95% confidence limit.

**Scheme 1.** Synthesis of 4,5-disubstituted 1-phenyl-1*H*-1,2,3-triazoles.

chlorination of their corresponding hydroxymethyl analogues (**13** and **14**) with thionyl chloride in dimethylformamide (DMF) (Scheme 1).

2.2. Affinities of 4,5-disubstituted 1-phenyl-1*H*-1,2,3-triazoles for $\beta 3$ and $\alpha 1\beta 2\gamma 2$ GABA receptors

The affinities of 4,5-disubstituted 1-(substituted phenyl)-1*H*-1,2,3-triazoles for human $\beta 3$ and $\alpha 1\beta 2\gamma 2$ receptors were evaluated by binding assays using [³H]EBOB as a radioligand. The obtained IC₅₀ values were converted to K_i values according to Cheng and Prusoff.²¹ The K_i values of disubstituted phenyltriazoles (**1**–**16**) for $\beta 3$ and $\alpha 1\beta 2\gamma 2$ receptors are listed in Table 1. All of the tested compounds, except **7**–**9**, showed affinity for $\beta 3$ receptors, whereas most of the compounds showed no or low affinity for $\alpha 1\beta 2\gamma 2$ receptors. Thus, most of the tested compounds showed higher affinity for $\beta 3$ receptors than for $\alpha 1\beta 2\gamma 2$ receptors. This is also the case for the 4- or 5-monosubstituted analogues (Table 2).¹⁹ Among the 4,5-disubstituted 1-phenyl-1*H*-1,2,3-triazoles with different alkyl substituents, the regioisomers

containing a long alkyl group at the 4-position of the triazole ring showed higher affinity for both $\beta 3$ and $\alpha 1\beta 2\gamma 2$ receptors than those containing a long alkyl group at the 5-position. This is consistent with our previous finding¹⁹ regarding the 4- or 5-monosubstituted phenyltriazoles that the 4-substituted regioisomer has higher affinity for receptors than the 5-substituted regioisomer (Table 2). 1-(2,6-Dichloro-4-trifluoromethylphenyl)-1*H*-1,2,3-triazoles containing an *n*-propyl group at the 4-position and a methyl (**4**), a hydroxymethyl (**13**), or a chloromethyl (**15**) group at the 5-position displayed the highest level of affinity for both $\beta 3$ and $\alpha 1\beta 2\gamma 2$ receptors. Replacement of the methyl group of **4** by a chloromethyl group at the 5-position to afford **15** resulted in only a ~3- and a ~1.2-fold enhancement in affinity for $\beta 3$ and $\alpha 1\beta 2\gamma 2$ receptors, respectively. This change in potency resulted in a 2.4-fold increase in selectivity for $\beta 3$ over $\alpha 1\beta 2\gamma 2$ receptors. When the methyl group was replaced by a hydroxymethyl group to give **13**, the affinity and selectivity of **13** remained almost the same as those of **4**. The affinity levels of **4**, **13**, and **15** were in the same range as those of 4-monosubstituted analogues

Table 2. Potencies of 1-(2,6-dichloro-4-trifluoromethylphenyl)-4 (or 5)-(alkyl or phenyl)-1*H*-1,2,3-triazoles in inhibiting [³H]EBOB binding to $\beta 3$ and $\alpha 1\beta 2\gamma 2$ GABA receptors

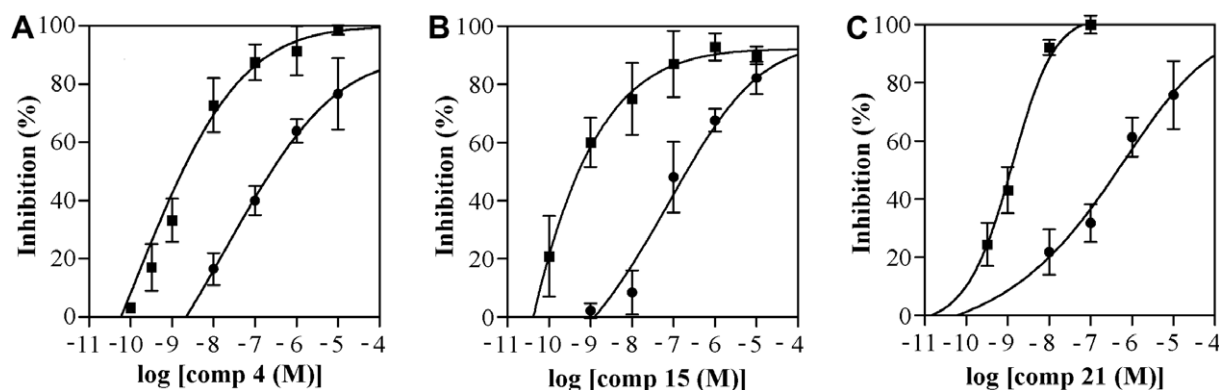
Compound	R ¹	R ²	K _i value		R _S ^b
			$\beta 3$ (nM) ^a	$\alpha 1\beta 2\gamma 2$ (μ M)	
17	<i>n</i> -Pr	H	2.14	0.470 (0.285–0.796 ^c)	220
18	H	<i>n</i> -Pr	757	>9.15	>12.1
19	<i>n</i> -Bu	H	2.79	1.01 (0.52–2.26 ^c)	362
21	<i>t</i> -Bu	H	0.831	0.390 (0.219–0.714 ^c)	470
23	<i>n</i> -Pen	H	27.8	1.39 (0.92–2.23 ^c)	50.0
24	H	<i>n</i> -Pen	1390	>9.15	>6.58
25	<i>n</i> -Hex	H	392	1.98 (1.21–3.62 ^c)	5.05
26	H	<i>n</i> -Hex	867	>9.15	>10.6
27	<i>c</i> -Hex	H	11.8	1.50 (0.84–3.07 ^c)	127
28	(CH ₂) ₃ Cl	H	1.63	0.616 (0.379–1.043 ^c)	378
29	Ph	H	128	>9.15	>71.5
30	H	Ph	475	>9.15	>19.3
31	Ph	NH ₂	20.3	1.16 (0.74–1.93 ^c)	57.1

Compounds with a K_i value of >8.00 μ M for $\beta 3$ receptors and a K_i value of >9.00 μ M for $\alpha 1\beta 2\gamma 2$ receptors: **20** (R¹ = H, R² = *n*-Bu) and **22** (R¹ = H, R² = *t*-Bu).

^a K_i values for $\beta 3$ receptors were calculated from IC₅₀ values reported in our previous paper¹⁹ according to Cheng and Prusoff.²¹

^b Selectivity for $\beta 3$ versus $\alpha 1\beta 2\gamma 2$ receptors (K_i ^{$\alpha 1\beta 2\gamma 2$} /K_i ^{$\beta 3$}).

^c 95% confidence limit.

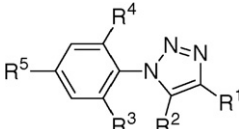
**Figure 2.** Concentration-inhibition curves of **4** (A), **15** (B), and **21** (C) in [³H]EBOB binding assays for human $\beta 3$ (■) and $\alpha 1\beta 2\gamma 2$ (●) GABA receptors. The data are means \pm SD for at least three experiments, each performed in duplicate.

with the highest levels of affinity, that is, the 4-*n*-propyl (**17**), the 4-*n*-butyl (**19**), the 4-*tert*-butyl (**21**), and the 4-chloropropyl (**28**) analogues (Table 2). Figures 2A and B show the dose–response curves of the two most active disubstituted phenyltriazoles (**4** and **15**) in $\beta 3$ and $\alpha 1\beta 2\gamma 2$ GABA receptors.

Compounds **10** and **12** were synthesized to examine the effect of increasing the length of the alkyl chain at the 5-position of **4**. The 4-*n*-propyl-5-ethyl analogue (**10**) showed a 4-fold decreased affinity for $\beta 3$ receptors and substantially lost affinity for $\alpha 1\beta 2\gamma 2$ receptors, which resulted in a >6-fold increase in selectivity compared to **4**, while the 4,5-dipropyl analogue (**12**) showed a ~66-fold decreased affinity for $\beta 3$ receptors and lost affinity for $\alpha 1\beta 2\gamma 2$ receptors, resulting in a <2-fold decreased selectivity. Replacement of the 4-*n*-propyl group of **4** by an ethyl group to produce the 4-ethyl-5-methyl analogue (**1**) led to a ~3-fold decreased affinity for both $\beta 3$ and

$\alpha 1\beta 2\gamma 2$ receptors and thus little change in selectivity. Replacement of the 5-methyl group of **1** by an ethyl group to give the 4,5-diethyl analogue (**3**) provided a ~2-fold increase in affinity for $\beta 3$ receptors, while the affinity for $\alpha 1\beta 2\gamma 2$ receptors remained almost unchanged.

Removal of chlorine atoms at the 2- and 6-positions of the phenyl group of **4** and **5** to give **8** and **9** resulted in substantial loss of affinity for both $\beta 3$ and $\alpha 1\beta 2\gamma 2$ receptors. Replacement of the chlorine atoms of **4** with bromine atoms gave **6** with a ~7-fold decreased affinity for $\beta 3$ receptors, although the selectivity increased <4-fold as the affinity for $\alpha 1\beta 2\gamma 2$ receptors was substantially lost. Taken together with the low potencies of **36–49** (Table 3), these findings indicate that the combination of 2,6-dichloro and 4-trifluoromethyl substitutions on the phenyl group of phenyltriazoles is important for high affinity for both $\beta 3$ and $\alpha 1\beta 2\gamma 2$ receptors, although regarding the selectivity, the bromo

Table 3. Potencies of 1-(2,4,6-trisubstituted phenyl)-4 (or 5)-*n*-butyl-1*H*-1,2,3-triazoles in inhibiting [³H]EBOB binding to $\beta 3$ and $\alpha 1\beta 2\gamma 2$ GABA receptors


Compound	R ¹	R ²	R ³ /R ⁴	R ⁵	K _i value		RS ^b
					$\beta 3$ (nM) ^a	$\alpha 1\beta 2\gamma 2$ (μ M)	
36	<i>n</i> -Bu	H	Cl	C \equiv CH	34.7	>9.15	>264
39	H	<i>n</i> -Bu	H	C \equiv CH	7580	>9.15	>1.21
40	<i>n</i> -Bu	H	Cl	Cl	82.3	>9.15	>111
41	H	<i>n</i> -Bu	Cl	Cl	4080	>9.15	>2.24
42	<i>n</i> -Bu	H	Cl	Br	31.2	>9.15	>293
43	H	<i>n</i> -Bu	Cl	Br	783	>9.15	>11.7
44	<i>n</i> -Bu	H	H	Br	3190	>9.15	>2.87
45	H	<i>n</i> -Bu	H	Br	2730	>9.15	>3.35
47	H	<i>n</i> -Bu	H	CF ₃	5300	>9.15	>1.73
48	<i>n</i> -Bu	H	Cl	H	3520	>9.15	>2.60
49	H	<i>n</i> -Bu	Cl	H	2050	>9.15	>4.46

Compounds with a K_i value of >8 μ M for $\beta 3$ receptors and a K_i value of >9 μ M for $\alpha 1\beta 2\gamma 2$ receptors (MCB: C \equiv C(CH₂)₂CO₂CH₃): **32** (R¹ = *n*-Bu, R² = H, R³/R⁴ = Cl, R⁵ = MCB), **33** (R¹ = H, R² = *n*-Bu, R³/R⁴ = Cl, R⁵ = MCB), **34** (R¹ = *n*-Bu, R² = H, R³/R⁴ = H, R⁵ = MCB), **35** (R¹ = H, R² = *n*-Bu, R³/R⁴ = H, R⁵ = MCB), **37** (R¹ = H, R² = *n*-Bu, R³/R⁴ = Cl, R⁵ = C \equiv CH), **38** (R¹ = *n*-Bu, R² = H, R³/R⁴ = H, R⁵ = C \equiv CH), and **46** (R¹ = *n*-Bu, R² = H, R³/R⁴ = H, R⁵ = CF₃).

^a K_i values for $\beta 3$ receptors were calculated from IC₅₀ values reported in our previous paper¹⁹ according to Cheng and Prusoff.²¹

^b Selectivity for $\beta 3$ versus $\alpha 1\beta 2\gamma 2$ receptors (K_i ^{$\alpha 1\beta 2\gamma 2$} /K_i ^{$\beta 3$}).

substitution at the 2- and 6-positions on the phenyl ring is preferable to the chloro substitution (**4** vs **6**). The rank orders of disubstituted phenyltriazoles to give high affinity for $\beta 3$ and $\alpha 1\beta 2\gamma 2$ receptors were the same as follows: 4-*n*-Pr, 5-CH₂Cl \geq 4-*n*-Pr, 5-Me \geq 4-*n*-Pr, 5-CH₂OH \geq 4,5-diEt \geq 4-Et, 5-Me \geq 4-*n*-Pr, 5-Et for $\beta 3$ receptors and 4-*n*-Pr, 5-CH₂Cl \geq 4-*n*-Pr, 5-Me \geq 4-*n*-Pr, 5-CH₂OH \geq 4,5-diEt \geq 4-Et, 5-Me \gg 4-*n*-Pr, 5-Et for $\alpha 1\beta 2\gamma 2$ receptors. The rank order of selectivity was as follows: 4-*n*-Pr, 5-Et \geq 4-*n*-Pr, 5-Me (2,6-Br₂-4-CF₃-Ph) > 4-*n*-Pr, 5-CH₂Cl > 4,5-diEt > 4-*n*-Pr, 5-Me > 4-*n*-Pr, 5-CH₂OH > 4-Et, 5-Me. Thus, the 4-*n*-propyl and 5-chloromethyl groups at the triazole ring of disubstituted phenyltriazoles are optimized substituents with respect to high affinity for $\beta 3$ receptors (K_i = 659 pM), but in terms of selectivity, the ethyl group is more effective than a chloromethyl group as the 5-substituent.

2.3. Affinities of 4- or 5-substituted 1-phenyl-1*H*-1,2,3-triazoles for $\beta 3$ and $\alpha 1\beta 2\gamma 2$ GABA receptors

As for the series of monosubstituted phenyltriazoles, their phenyl or alkyl groups at the 4- or 5-position of the triazole ring were examined for their effects on the affinities for $\alpha 1\beta 2\gamma 2$ GABA receptors. Table 2 is the list of the K_i values of 4- or 5-substituted 1-(2,6-dichloro-4-trifluoromethylphenyl)-1*H*-1,2,3-triazoles, including the previously reported data¹⁹ for $\beta 3$ GABA receptors for comparison. The binding affinity data revealed that the affinity of the 4-regioisomers is higher than that of the 5-regioisomers in every case. Most of the monosubstituted analogues of 1-(2,6-dichloro-4-trifluoromethylphenyl)-1*H*-1,2,3-triazoles exhibited higher affinity for $\beta 3$ receptors than for $\alpha 1\beta 2\gamma 2$ receptors. Among the mono-

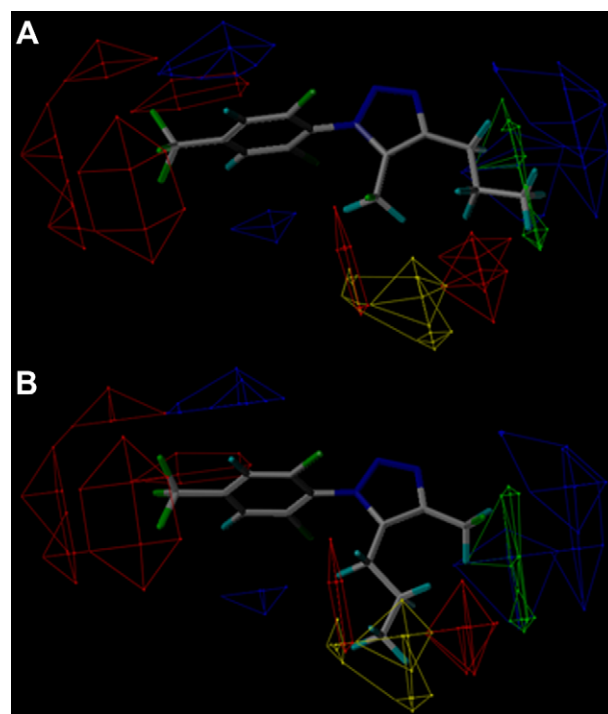


Figure 3. CoMFA contour plots for a human $\beta 3$ GABA receptor model. The green contours indicate areas where sterically bulky substituents increase receptor affinity, whereas the yellow contours indicate areas where sterically bulky groups are detrimental to the potency. The blue contours indicate areas where electropositive groups enhance affinity for receptors, while the red contours represent areas where electronegative moieties are favorable for receptor affinity. Compounds **15** and **16** are shown as reference molecules in (A) and (B), respectively.

substituted phenyltriazoles, the 4-*tert*-butyl analogue (**21**) showed the highest affinity for both $\beta 3$ ($K_i = 831$ pM) and $\alpha 1\beta 2\gamma 2$ ($K_i = 390$ nM) receptors and a 470-fold selectivity for $\beta 3$ versus $\alpha 1\beta 2\gamma 2$ receptors. Figure 2C shows the dose–response curves of this highly active, selective phenyltriazole. Replacement of the 4-*tert*-butyl group of **21** with a C3–C6 unbranched alkyl group or a phenyl group resulted in decreased affinity in the following order: *t*-Bu > *n*-Pr \geq *n*-Bu > *n*-Pen > Ph > *n*-Hex for $\beta 3$ receptors and *t*-Bu \geq *n*-Pr \geq *n*-Bu \approx *n*-Pen > *n*-Hex \gg Ph for $\alpha 1\beta 2\gamma 2$ receptors. The selectivity for $\beta 3$ versus $\alpha 1\beta 2\gamma 2$ receptors was as follows: *t*-Bu > *n*-Bu > *n*-Pr > Ph \geq *n*-Pen > *n*-Hex. These findings indicate that long alkyl chains do not conform to the binding site in either $\beta 3$ or $\alpha 1\beta 2\gamma 2$ receptors. Replacement of the 4-phenyl group of **29** by a cyclohexyl group to give **27** led to a ~ 11 -fold and a >6-fold increase in affinity for $\beta 3$ and $\alpha 1\beta 2\gamma 2$ receptors, respectively. Introduction of an amino group into the 5-position of the triazole ring of **29** to afford **31** resulted in ~ 6 -fold and >8-fold enhancements in affinity for $\beta 3$ and $\alpha 1\beta 2\gamma 2$ receptors, respectively. When the distal-end methyl group of the 4-*n*-butyl group of **19** was replaced with a chlorine atom to produce the 4-*n*-chloropropyl analogue (**28**), the analogue did not exhibit a marked increase in either affinity or selectivity. Taken together, these findings indicate that the *tert*-butyl group at the 4-position of the triazole ring is an optimum substituent in terms of both high potency for $\beta 3$ receptors and selectivity for $\beta 3$ versus $\alpha 1\beta 2\gamma 2$ receptors, followed by the chloropropyl and *n*-propyl groups.

2.4. CoMFA and CoMSIA 3D-QSAR models

We performed 3D-QSAR analyses to predict the favorable and unfavorable moieties of 1-phenyl-1*H*-1,2,3-phenyltriazoles for high potency in $\beta 3$ receptors using the CoMFA (comparative molecular field analysis)²² and CoMSIA (comparative molecular similarity indices analysis)²³ modules in the SYBYL program. 3D-QSAR analyses such as CoMFA and CoMSIA are generally applied to find the common features of ligands that are important for binding to receptors, and the information obtained is usually used to design and develop novel ligands. Both analyses are based on the assumption that changes in the binding affinities of ligands are related to changes in different fields surrounding the molecules, such as the steric and electrostatic fields, as well as the hydrophobic properties and hydrogen-bond accepting and donating capabilities. The partial least squares (PLS) analysis is a multivariate statistical method that is used to generate QSAR and can be applied for predicting the binding affinity of ligands. The CoMFA methodology was first introduced by Cramer et al.,²² and CoMSIA is an extension of the CoMFA method reported by Klebe et al.²³ The difference between these two methods is in the implementation of the fields. In most cases the predictive ability of CoMSIA is the same or better than, or complementary to that of CoMFA.^{24–26}

3D-QSAR studies were conducted successfully only on $\beta 3$ GABA receptors. Those on $\alpha 1\beta 2\gamma 2$ GABA receptors

failed to give appropriate contour maps, although the cross-validated and non-cross-validated predictive abilities were statistically significant in both analyses (data not shown). The reason why we failed to obtain good contour plots in the case of $\alpha 1\beta 2\gamma 2$ receptors might be the low receptor affinity of all active compounds and the narrow range of the K_i values. To generate a CoMFA model for $\beta 3$ receptors, we first used 37 active phenyltriazoles in the analysis. The cross-validated (q^2) and non-cross-validated (r^2) correlation coefficients were 0.508 and 0.709, respectively. In this analysis, as the differences between the predictive and actual pK_i ($-\log K_i$) values of four compounds (**14**, **25**, **44**, and **48**) were more than one logarithmic unit, these compounds were omitted from the final analysis. Although the reason why such compounds showed a large deviation is not clear at this moment, it should be noted that they all are analogues with low potency. The summary of the final CoMFA results is shown in Table 4. The cross-validated and non-cross-validated correlation coefficients were 0.705 and 0.854, respectively. The standard error of prediction (s_{press}) and the standard error of estimate (s) were 0.677 and 0.476 for leave-one-out cross-validated and non-cross-validated analysis, respectively. The cross-validated correlation coefficient is a better criterion to judge the model quality than the non-cross-validated correlation coefficient, and the above high q^2 value indicates the validity of the suggested mode of interaction of phenyltriazoles with $\beta 3$ receptors.

The CoMFA steric and electrostatic field contour maps for $\beta 3$ receptors are shown in Figure 3. The green contours indicate areas where sterically bulky substituents increase receptor affinity, whereas the yellow contours indicate areas where sterically bulky groups are detrimental to the potency. The blue contours indicate areas where electropositive groups enhance affinity for receptors, while the red contours represent areas where electronegative moieties are favorable for receptor affinity. The finding that the activities of **4**, **13**, **15**, **17**, and **21** are higher than those of their corresponding regioisomers is due to the fact that the *n*-propyl or the *tert*-butyl group at the 4-position of the triazole ring occupies the green contours, whereas the *n*-propyl or the *tert*-butyl group at the 5-position of the same ring interacts with the yellow contours. The phenyltriazoles containing a long substituent(s) at either the 4-, 5-, or both position(s), such as compounds **12**, **23**, **24**, **26**, **29**, and **30**, showed low affinity due to the fact that the substituents occupy the yellow contours. The red contours around the 4-position of the benzene ring indicate that a more negatively charged group at this site would enhance the receptor affinity. Compounds (e.g., **48**) without an electronegative substituent at the 4-position of the phenyl ring or compounds (e.g., **36**, **40**, and **42**) that have a lower electronegative substituent (e.g., $\text{C}\equiv\text{CH}$, Cl, and Br) than a trifluoromethyl group showed lower activity than **19**, which has a trifluoromethyl group at this position. Blue contours that appeared above and below the benzene ring indicate that a more positive charge is preferred on the benzene ring. Thus, the strong electron-withdrawing substituents at the 2-, 4-, and

Table 4. Results of CoMFA and CoMSIA of 1-phenyl-1*H*-1,2,3-triazole binding to $\beta 3$ GABA receptors $pK_i = a + [\text{CoMFA or CoMSIA field terms}]$

Analysis	<i>a</i>	<i>C</i> ^a	<i>n</i>	<i>s</i>	<i>r</i> ²	<i>F</i> _{c,n-c-1}	Cross-validated		Relative contribution		
							<i>s</i> _{press}	<i>q</i> ²	<i>S</i> ^b	<i>E</i> ^c	<i>H</i> ^d
CoMFA	6.928	2	33	0.476	0.854	87.755	0.677	0.705	0.694	0.306	—
CoMSIA	6.601	5	35	0.332	0.936	84.787	0.757	0.668	0.262	0.465	0.273

Compounds **14**, **25**, **44**, and **48** were excluded in CoMFA, and **14** and **48** were omitted in CoMSIA.

^a Optimum component.

^b Steric.

^c Electrostatic.

^d Hydrophobic.

6- positions of the phenyl group might make the charge distribution on the benzene ring relatively electropositive. This is consistent with the observation that phenyltriazoles (e.g., **38**, **44**, **46**, or **48**) without electronegative atoms at the 2-, 4-, or 6-position on the benzene ring or those (e.g., **6**) having substituents with less electron-withdrawing ability at these positions led to a decrease or loss of affinity for receptors compared to their corresponding analogues. It is interesting to note that red contours are present between the 4- and 5-substituents of the triazole ring. The negative electrostatic regions at this position probably arise due to the fact that several phenyltriazoles, such as **13**, **15**, **28**, and **31**, contain electronegative substituents at either the 4- or 5-position of the triazole ring. The 3-chloropropyl group of **28** is acceptable as the *n*-butyl group of **19**, and the introduction of an amino group into the 5-position of **29** to produce **31** also led to increased receptor affinity, as the electronegative substituents probably occupy the electronegatively favorable regions. These findings allow us to speculate that an appropriate electronegative substituent at these positions would increase receptor affinity.

It is generally thought that molecular alignment changes exert less effect on the results in CoMSIA, which also affords smoother and more easily interpretable contour plots using Gaussian type distance dependence with the molecular similarity indices in the analysis.²³ In addition to the steric and electrostatic fields of CoMFA, CoMSIA also defines clear hydrophobic and hydrogen-bond donor/acceptor descriptor fields. In the present CoMSIA PLS analysis, we considered steric, electrostatic, and hydrophobic field descriptors to obtain a $\beta 3$ receptor model, since most of the substituents of our compounds contain no hydrogen-bond donor or acceptor atom. Thirty-seven active phenyltriazoles were used to generate a CoMSIA $\beta 3$ receptor model, and two compounds (**14** and **48**) showed a large deviation from this model and were excluded in the final analysis. The excluded compounds are the compounds that also showed a large deviation in the CoMFA. The reason for the large deviation is obscure at this time. The results of the final CoMSIA are summarized in Table 4. The leave-one-out cross-validated PLS analysis coefficient (*q*²) was 0.668, and the standard error of prediction (*s*_{press}) was 0.757. The optimum number of components obtained from the cross-validation linear regression coefficient was used to produce the non-cross-validated model. The non-cross-validated PLS analysis yielded a high correlation coefficient (*r*²) of 0.936 with a low standard error estimate (*s*) of 0.332.

The CoMSIA steric and electrostatic stdev * coefficient contour plots obtained from non-cross-validated PLS analysis are shown in Figures 4A and B, respectively. The green contours indicate regions where sterically bulky substituents are favorable, while the yellow contours show regions where sterically bulky substituents are unfavorable for receptor affinity. The blue contours indicate areas where electropositive groups enhance receptor affinity in this region, while the interaction of electronegative substituents with areas shown with red contours increases affinity. Information obtained from CoMSIA contour maps (Fig. 4A) was similar to that obtained from CoMFA contour maps with respect to steric effects, but one exception was also noted. The CoMSIA contour indicates that there is another sterically disfavored region located behind the sterically favored regions indicated by the green contours around the 4-position of the triazole ring, whereas this region was not observed in the CoMFA model. This finding indicates that optimum sizes of substituents for affinity for receptors are present at both 4- and 5-positions. The electrostatic contour map of CoMSIA (Fig. 4B) was comparable to that of CoMFA (Fig. 3) with a few exceptions. A small red contour between the 4- and 5-positions of the triazole ring in CoMFA turned into two large linked red contours in CoMSIA, and the red contours around the trifluoromethyl group at the 4-position of the benzene ring became smaller. CoMSIA predicts that the contribution of electronegative substituents to the binding affinity at the 4- and 5-positions of the triazole ring is high, while the contribution of the electronegative substituent at the 4-position of the benzene ring is low. The electronegative groups of compounds **13**, **15**, **16**, and **28–31** at the 4- or 5-position of the triazole ring might have contributed to the generation of red contours that are present near the triazole ring.

The CoMSIA hydrophobic field map is shown in Figure 4C. The yellow contours in this figure represent hydrophobic favorable regions that enhance the affinity for receptors, while the white contours show hydrophobic unfavorable regions. Several favorable and unfavorable regions appeared in the hydrophobic property contour map. The presence of yellow contours behind the white contour around the 4-position of the triazole ring indicates that an optimum hydrophobicity of substituents for high potency is present at this position. At the same time, the presence of a yellow contour in front of the white contour at the 5-position of the triazole ring indicates that small rather than large hydrophobic

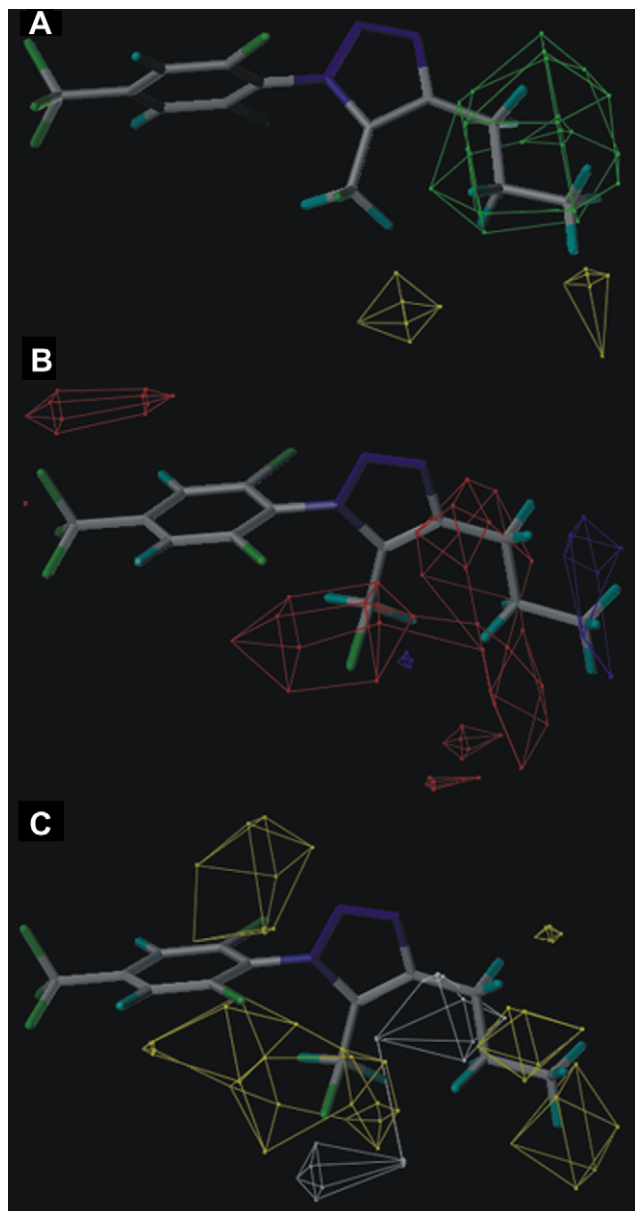


Figure 4. CoMSIA model for the human β_3 GABA receptor. (A) Steric contour plots. The green contours indicate regions where sterically bulky substituents are favorable, while the yellow contours show regions where sterically bulky substituents are unfavorable for receptor affinity. (B) Electrostatic contour plots. The blue contours indicate regions where the electropositive groups enhance receptor affinity, while the interaction of electronegative substituents with the areas indicated by red contours increases affinity. (C) Hydrophobic contour plots. The yellow contours in this figure indicate hydrophobic favorable regions that enhance the affinity for receptors, while the white contours show hydrophobic unfavorable regions. Compound **15** is shown as a reference molecule.

substituents are favorable for high affinity at this position. A hydrophobic substituent of excessive length is not favorable at the 4-position of the triazole ring, because the sterically unfavorable region (Fig. 4A) is located behind the hydrophobic favorable region (Fig. 4C). The two other yellow contours above and below the benzene ring indicate that the hydrophobic nature of the benzene ring would increase the receptor affinity, which could be achieved by introducing electro-

negative substituents at the 2-, 4-, and 6-positions of the phenyl ring. This finding could explain that there was low or no activity of phenyltriazoles having low electronegative substituents or of phenyltriazoles without substituents at the 2-, 4-, and 6-positions of the benzene ring.

Both CoMFA and CoMSIA provided consistent PLS statistical results and contour maps for β_3 receptors, with only a few exceptions. In CoMSIA, a higher non-cross-validated correlation coefficient (r^2) and a lower standard error of estimate (s) were obtained than in CoMFA, although the cross-validated correlation coefficient (q^2) and the standard error of prediction (s_{press}) were almost similar. Regarding the relative field contributions, the CoMFA results showed that steric fields made greater contributions to the affinity of compounds than electrostatic fields, whereas the CoMSIA results showed that electrostatic fields made a greater contribution than steric and hydrophobic fields. It is also noted that the steric and hydrophobic field contributions were almost the same in CoMSIA. CoMSIA apparently performed better to explain the structure–activity relationships of phenyltriazoles in β_3 receptors than CoMFA, because of additional information on the hydrophobic field in the 3D-QSAR model.

2.5. Binding sites and selectivity of 1-phenyl-1*H*-1,2,3-triazoles for β_3 over $\alpha 1\beta 2\gamma 2$ GABA receptors

We performed homology modeling studies of human β_3 and $\alpha 1\beta 2\gamma 2$ GABA receptors in an attempt to predict the binding site of 1-phenyl-1*H*-1,2,3-triazoles as well as to find out the cause of their selectivity for β_3 over $\alpha 1\beta 2\gamma 2$ receptors. The homology models were built using an atomic model of the closed nicotinic acetylcholine receptor channel, resolved to 4 Å by electron microscopy of the crystalline postsynaptic membrane of *Torpedo marmorata*²⁷ as a template. Both GABA and nicotinic acetylcholine receptors belong to a Cys-loop receptor family of ligand-gated ion channels that share structural features; for example, they consist of five subunits, each of which has four α -helical trans-membrane segments (TM1–TM4). The TM2s from the five subunits are assembled to form a channel lumen. The amino acid sequences of TM2 of GABA receptor subunits are shown in Figure 5A. The subunit correspondence of the $\alpha 1\beta 2\gamma 2$ receptor to the nicotinic acetylcholine receptor is depicted in Figure 5B. Figure 6A shows amino acids from the 2' to 6' position of the TM2 channel lumen of the homology model of the human β_3 homopentamer with **15**, one of the most active analogues, automatically docked using the chemistry and bioinformatics package MOE. The T6' methyl groups of the homopentamer show favorable hydrophobic interactions with the *n*-propyl group of the 4-position of the triazole ring, and one of the A2' methyl groups of the homopentamer shows favorable hydrophobic interactions with the phenyl group. The T6' hydroxyl group probably forms hydrogen bonds with the nitrogen atoms of the 2- and 3-positions of the triazole ring. Introduction of an alkyl chain longer than the *n*-propyl group or a substituent bulkier than the *tert*-butyl

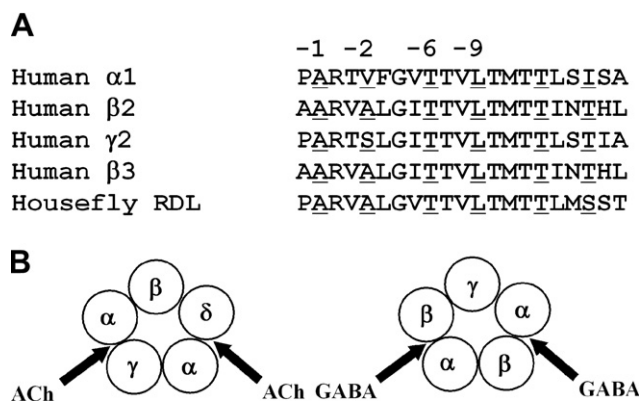


Figure 5. Amino acid sequences of the putative binding site and subunit correspondence. (A) Amino acid residues of TM2 of GABA receptor subunits. Pore-facing amino acids are underlined. Accession Nos. human $\alpha 1$ subunit = NM_174540; human $\beta 2$ subunit = NM_000813; human $\gamma 2$ subunit = NM_000816; human $\beta 3$ subunit = NM_000814; housefly RDL subunit = AB177547. The positions of amino acid residues are index-numbered from the N-terminal side of TM2 according to Miller.⁴⁶ (B) Schematic presentation of subunit correspondence between the nicotinic acetylcholine receptor and the $\alpha 1\beta 2\gamma 2$ GABA receptor. Agonist binding sites are indicated by arrows.

group at the 4-position of the triazole ring would result in a collision with the channel wall, which would make the compounds less potent than the parent compound, as predicted in 3D-QSAR studies. Most of the compounds performed similar interactions with the putative binding site within the channel pore, whereas some of the compounds (**6**, **13**, and **17**) were docked into a different binding site or in a different orientation. For instance, the 2,6-dibromo-4-trifluoromethylphenyl group of **6** was involved in hydrophobic interactions with the T6' and L9' methyl groups, and the 5-methyl-4-*n*-propyl-1*H*-1,2,3-triazole moiety was outside the putative binding site. The 4-*n*-propyl group of **17** was involved in hydrophobic interactions with the T6' and L9' methyl groups, and the 2,6-dichloro-4-trifluoromethylphenyl group was outside the putative binding site. The reason why these compounds bound to the different sites is uncertain at the present moment. The refinement of

our homology model will be needed so as to incorporate all analogues into the model.

It has been shown that a β subunit is essential for the binding of non-competitive antagonists to heteromeric GABA_A receptors, and that the $\beta 3$ subunit alone can form a channel that is sufficient for antagonist binding.^{16,28} It is believed that the binding site for non-competitive antagonists is located within the channel pore. Recent site-directed mutagenesis studies of various GABA_A receptors have reported on the molecular localization of the antagonist binding site, and the amino acid residues responsible for the binding have been shown to exist in the cytoplasmic half of TM2 of the channels.^{29–35} On the basis of site-directed mutagenesis and molecular modeling results of the $\beta 3$ homopentamer, Chen et al. reported with reference to information from other studies that widely diverse non-competitive antagonists bind to the same site of the receptor, and pointed out that A2' and T6' play important roles for antagonist binding, with L9' playing a supplemental role.³⁵ In another model of the $\beta 3$ receptor provided by Ci et al., L3', A2', and T6' were postulated to play more important roles than L9' for interaction with fipronil-related non-competitive antagonists.³⁶ The A2'S mutation of $\beta 3$ receptors caused a reduced affinity for EBOB binding, whereas the T6'V mutation abolished the binding, which indicates that the 6' amino acid has more intense effects than the 2' amino acid on EBOB binding to these receptors.³⁷ Even if the findings regarding the putative binding site in our model are mostly consistent with these other research results, it should be noted that different binding orientations from those of fipronil and its related antagonists were observed for 1-phenyl-1*H*-1,2,3-triazole antagonists.^{35,36} Fipronil and its closely related analogues showed levels of potency almost identical to those of the GABA receptors obtained from *Rdl* (A2'S) mutant and wild-type houseflies, whereas the 4-*tert*-butyl analogue of phenyltriazole (**21**) showed lower affinity for the GABA receptors of *Rdl* mutant houseflies than for those of wild-type houseflies.³⁸ The alkyl group at the 4-position of the triazole ring of phenyltriazoles and the trifluoromethylsulfinyl group of fipronil are different in terms of electron density,¹⁹ which

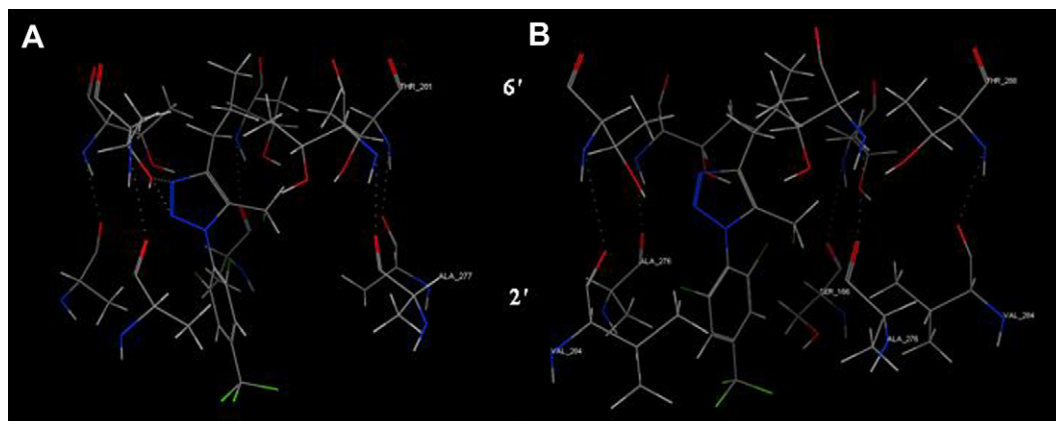


Figure 6. Docking of 1-phenyl-1*H*-1,2,3-triazoles into GABA receptors. Compound **15** was automatically docked into (A) homopentameric $\beta 3$ receptors and (B) heteropentameric $\alpha 1\beta 2\gamma 2$ receptors.

might be responsible for the binding of fipronil to $\beta 3$ receptors in a different orientation. A definitive conclusion regarding the binding orientation of antagonists must await a high-resolution characterization of the structure of ligand-gated ion channels.

The channel lumen from the 2' to 6' position of the homology model of the human $\alpha 1\beta 2\gamma 2$ heteropentamer is shown in Figure 6B, and the most active compound (**15**) was docked into the putative binding site. Favorable hydrophobic contacts were observed for the T6' methyl groups with the alkyl substituent at the 4-position of the triazole ring and for the V2' and A2' methyl groups with the 2,6-dichloro-4-trifluoromethylphenyl group. All of the compounds except **25** displayed the same binding orientation within the channel pore. The long *n*-hexyl group of **25** was involved in hydrophobic interactions with the V2' and T6' methyl groups and the triazole ring with the L9' methyl groups, and the 2,6-dichloro-4-trifluoromethylphenyl group resided outside the putative binding site. Perret et al. reported that a major interaction of chemically reactive phenylpyrazole antagonists occurred at the V257 position of rat $\alpha 1$ subunit,³¹ which is equivalent to the V2' position of human $\alpha 1$ subunit (Fig. 5A). The same amino acid had been suggested to be involved in binding the antagonist picrotoxinin by the substituted-cysteine accessibility method.²⁹ Recombinant rat $\alpha 1\beta 2\gamma 2$ receptors containing the T6'F mutation in the $\alpha 1$, $\beta 2$, or $\gamma 2$ subunit were shown to be insensitive to picrotoxinin.³⁰ The results of our docking studies are in agreement with those of these site-directed mutagenesis studies.

How can we explain the selectivity of 1-phenyl-1*H*-1,2,3-triazoles for $\beta 3$ over $\alpha 1\beta 2\gamma 2$ receptors? The $\beta 3$ GABA receptor is a homopentamer in which the channel-lining pores at the 2' and 6' positions are formed by only alanine and threonine residues, respectively, thereby making the channel lumen symmetrical, so any parallel alignment of phenyltriazoles to the channel pore axis at this putative binding site might be favorable for hydrophobic interactions and for the formation of hydrogen bonds between the hydroxyl group of T6' and the nitrogen atoms of the triazole ring of **15**. In contrast, the channel-lining pore at the 2' position of the heteropentameric $\alpha 1\beta 2\gamma 2$ GABA receptor is formed by two valines, two alanines, and one serine residue, which makes the channel pore unsymmetrical. Therefore, the specific alignment of phenyltriazoles in the channel pore might be necessary for favorable hydrophobic interaction with the V2' and A2' methyl groups. The docking energy of **15** in $\beta 3$ receptors was found to be lower (−5.66 kcal/mol) than that in $\alpha 1\beta 2\gamma 2$ receptors (−4.26 kcal/mol), and similar relations were also observed for other analogues, indicating that 1-phenyl-1*H*-1,2,3-triazoles are more stable in $\beta 3$ receptor channels than in $\alpha 1\beta 2\gamma 2$ GABA receptor channels. The higher docking energy in $\alpha 1\beta 2\gamma 2$ receptors might be due to the steric repulsion of the bulky isopropyl side chain of V2' with the phenyl groups of 1-phenyl-1*H*-1,2,3-triazoles, which also keeps the triazole ring far from the hydroxyl groups of T6' and thereby prevents the formation of hydrogen bonds in the case of **15**. This factor

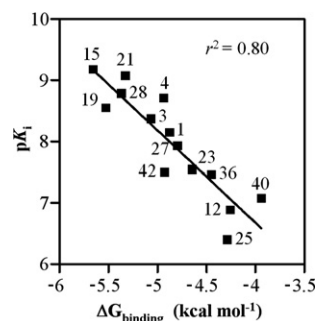


Figure 7. Correlation between the total binding energy ($\Delta G_{\text{binding}}$) determined by docking studies and the experimentally determined affinity (pK_i) of 1-phenyl-1*H*-1,2,3-triazoles for human $\beta 3$ GABA receptors. Compound numbers are indicated.

would make the molecules less stable in the channel pore of $\alpha 1\beta 2\gamma 2$ receptors than in that of $\beta 3$ receptors. This might be one of the reasons that 1-phenyl-1*H*-1,2,3-triazoles select $\beta 3$ over $\alpha 1\beta 2\gamma 2$ GABA receptors.

Finally, to validate the suggested mode of interaction between 1-phenyl-1*H*-1,2,3-triazoles and the homology model of human $\beta 3$ receptors, we examined the relationship between the total binding energies ($\Delta G_{\text{binding}}$) calculated by the MOE program and the experimentally determined affinity (pK_i) values. We first randomly chose 17 analogues for this validation so as to include compounds with a broad range of potency ($K_i = 0.659$ –392 nM). As a result, a good correlation ($r^2 = 0.80$) was obtained between $\Delta G_{\text{binding}}$ and the pK_i values of 14 selected 1-phenyl-1*H*-1,2,3-triazoles with a wide range of potency (Fig. 7), although three compounds (**6**, **13**, and **17**) that failed to bind to the 2' and 6' positions were omitted from the plot for the reason that most of the site-directed mutagenesis studies using GABA and glycine receptors identified the 2' and 6' amino acids as amino acids responsible for antagonist binding. Further, we tested three more compounds (**10**, **29**, and **31**) to see whether the addition of these compounds deteriorates the correlation, and this addition did not significantly affect the correlation. This finding indicates the validity of our model. As for $\alpha 1\beta 2\gamma 2$ receptors, a plot of $\Delta G_{\text{binding}}$ values against pK_i values yielded a correlation ($r^2 = 0.77$) for 8 compounds (**15**, **17**, **21**, **23**, **25**, **27**, **28**, and **31**), although only a limited number and a narrow range of pK_i values for 1-phenyl-1*H*-1,2,3-triazoles were available (plot not shown).

2.6. Conclusions

In the current study, we synthesized a series of 4,5-disubstituted 1-phenyl-1*H*-1,2,3-triazoles and examined their antagonist potencies (affinities) in human $\beta 3$ and $\alpha 1\beta 2\gamma 2$ GABA receptors to study the structure–activity relationships. Compound **15** exhibited the highest level of affinity for both $\beta 3$ and $\alpha 1\beta 2\gamma 2$ receptors, which was the same level as that of the most potent monosubstituted analogue (**21**). Most of the analogues were more potent in $\beta 3$ receptors than in $\alpha 1\beta 2\gamma 2$ receptors. The 4-*n*-propyl-5-ethyl analogue (**10**) exhibited the highest selectivity. The *n*-propyl group at the 4-position and the chloromethyl group at the 5-position of

1-(2,6-dichloro-4-trifluoromethylphenyl)-1*H*-1,2,3-triazole are optimum substituents with respect to conferring high affinity for $\beta 3$ receptors (K_i = 659 pM), but in terms of selectivity for $\beta 3$ versus $\alpha 1\beta 2\gamma 2$ receptors, the ethyl group ($RS > 1133$ -fold) is preferable to the chloromethyl group as the 5-substituent. 3D-QSAR studies revealed that a small hydrophobic 4-substituent and a hydrophobic or hydrophilic 5-substituent smaller than the 4-substituent are favorable for high potency at $\beta 3$ receptors, together with electronegative substituents at the 2-, 4-, and 6-positions on the benzene ring. Docking studies using a $\beta 3$ GABA receptor homology model showed that the amino acid residues at the 2'- and 6'-positions play an important role in binding 1-phenyl-1*H*-1,2,3-triazoles. The flexibility of the alignment of molecules in the channel lumen and a specific hydrophobic environment at the 2'-position of $\beta 3$ homopentamers that are brought about by the composition of the same five subunits could be one of the reasons that 1-phenyl-1*H*-1,2,3-triazoles select $\beta 3$ over $\alpha 1\beta 2\gamma 2$ receptors.

The K_i values of compounds such as **4**, **13**, **15**, **17**, **21**, and **28** in the range of 0.66 to 2.53 nM in $\beta 3$ receptors are comparable to or smaller than the reported IC_{50} values of the GABA receptor antagonist/commercial insecticide fipronil^{14,16,39,40} and those of its 4-*tert*-butyl and 4-isopropyl analogues in $\beta 3$ or native housefly receptors.¹⁷ The interaction of 1-phenyl-1*H*-1,2,3-triazoles with housefly GABA receptors causes significant insecticidal activity,¹⁹ and the most two potent analogues (**15** and **21**) demonstrated considerable insecticidal activity (LD_{50} s = 5.17 and 1.86 pmol/fly,¹⁹ respectively) against houseflies. The information obtained from the 3D contour maps of CoMFA and CoMSIA of $\beta 3$ receptors together with the homology models of $\beta 3$ and $\alpha 1\beta 2\gamma 2$ receptors should prove helpful for understanding the mechanisms of the interaction of non-competitive antagonists with GABA receptors, and might afford useful information for designing new insect control chemicals.

3. Experimental

3.1. Synthesis

3.1.1. General. ¹H NMR spectra were obtained on a JEOL JNM-A 400 spectrometer, and chemical shifts (δ values) are given in ppm using tetramethylsilane (TMS) as an internal standard. Mass spectra were taken on a Hitachi M80-B spectrometer using the electron impact method (70 eV), and the fragment data are reported as m/z . Melting points were determined using a Yanagimoto MP 500D apparatus and are uncorrected. [Propyl-2,3-³H]EBOB (47.5 or 45.0 Ci/mmol) was purchased from Perkin-Elmer Life Sciences, Inc. (Boston, MA). Phenyltriazoles **17–49** were available from our earlier studies.^{18,19} General chemicals were purchased from Wako Pure Chemical Industries, Ltd (Osaka, Japan) unless otherwise noted.

3.1.2. General procedure for the synthesis of 4,5-disubstituted 1-phenyl-1*H*-1,2,3-triazoles (Scheme 1). The procedure for synthesis of disubstituted phenyltriazoles was the

same as that described in our previous paper.¹⁹ Briefly, 2,6-dichloro-4-trifluoromethylphenyl azide was prepared from 2,6-dichloro-4-trifluoromethylaniline (670 mg, 2.91 mmol) by the treatment with concd HCl (50 mL), sodium nitrite (200 mg, 2.91 mmol), and sodium azide (190 mg, 2.91 mmol) in water (50 mL), and the mixture was stirred overnight at room temperature. After completion of the reaction, the mixture was extracted with CH_2Cl_2 , and the solvent was evaporated. The residue was chromatographed on silica gel (*n*-hexane), affording 2,6-dichloro-4-trifluoromethylphenyl azide as a red oil. 2,6-Dichloro-4-trifluoromethylphenyl azide (600 mg, 2.38 mmol), an unsymmetrical alkyne (2.38 mmol), and toluene (3 mL) were placed in a sealed tube and heated at 110 °C for 16 h. After the reaction, the mixture was partitioned between water and ether. The ether layer was dried with sodium sulfate overnight. The ether was evaporated, and the residue was subjected to silica gel column chromatography (*n*-hexane/EtOAc = 30:1), thus affording the 4,5-dialkyl isomers of the desired compound. Compounds **1–14** were synthesized by this method.

3.1.3. 1-(2,6-Dichloro-4-trifluoromethylphenyl)-4-ethyl-5-methyl-1*H*-1,2,3-triazole (1). Yield 23%, mp 71.2–72.1 °C. ¹H NMR ($CDCl_3$) δ 1.37 (3H, t, J = 7.6 Hz, CH_2CH_3), 2.77 (2H, q, J = 7.6 Hz, CH_2CH_3), 2.11 (3H, s, CH_3), 7.78 (2H, s, Ph). EIMS m/z (%) 41 (100), 240 (34), 280 (82), 283 (55), 323 (M, 8), 325 (M+2, 5). Anal. Calcd for $C_{12}H_{10}Cl_2F_3N_3$: C, 44.47; H, 3.11; N, 12.96%. Found: C, 44.73; H, 3.20; N, 12.66%.

3.1.4. 1-(2,6-Dichloro-4-trifluoromethylphenyl)-5-ethyl-4-methyl-1*H*-1,2,3-triazole (2). Yield 17%, mp 64.6–65.7 °C. ¹H NMR ($CDCl_3$) δ 1.08 (3H, t, J = 7.6 Hz, CH_2CH_3), 2.51 (2H, q, J = 7.6 Hz, CH_2CH_3), 2.42 (3H, s, CH_3), 7.78 (2H, s, Ph). EIMS m/z (%) 41 (100), 280 (80), 282 (53), 323 (M, 3.2), 325 (M+2, 2.2). Anal. Calcd for $C_{12}H_{10}Cl_2F_3N_3$: C, 44.47; H, 3.11; N, 12.96%. Found: C, 44.83; H, 3.29; N, 12.50%.

3.1.5. 1-(2,6-Dichloro-4-trifluoromethylphenyl)-4,5-diethyl-1*H*-1,2,3-triazole (3). Yield 37%, mp 68.9–69.6 °C. ¹H NMR ($CDCl_3$) δ 1.07 (3H, t, J = 7.7 Hz, CH_2CH_3 -5), 1.38 (3H, t, J = 7.6 Hz, CH_2CH_3 -4), 2.51 (2H, q, J = 7.7 Hz, CH_2CH_3 -5), 2.78 (2H, q, J = 7.6 Hz, CH_2CH_3 -4), 7.78 (2H, s, Ph). EIMS m/z (%) 294 (100), 309 (11), 337 (M, 3), 339 (M+2, 2). Anal. Calcd for $C_{13}H_{12}Cl_2F_3N_3$: C, 46.17; H, 3.58; N, 12.43%. Found: C, 46.17; H, 3.62; N, 12.11%.

3.1.6. 1-(2,6-Dichloro-4-trifluoromethylphenyl)-5-methyl-4-*n*-propyl-1*H*-1,2,3-triazole (4). Yield 40%, oily liquid. ¹H NMR ($CDCl_3$) δ 0.98 (3H, t, J = 7.3 Hz, $(CH_2)_2CH_3$), 1.79 (2H, sex, J = 7.3 Hz, $CH_2CH_2CH_3$), 2.10 (3H, s, CH_3), 2.72 (2H, t, J = 7.3 Hz, $CH_2CH_2CH_3$), 7.78 (2H, s, Ph). EIMS m/z (%) 280 (100), 282 (65), 337 (M, 6), 339 (M+2, 4). Anal. Calcd for $C_{13}H_{12}Cl_2F_3N_3$: C, 46.17; H, 3.58; N, 12.43%. Found: C, 46.32; H, 3.56; N, 12.15%.

3.1.7. 1-(2,6-Dichloro-4-trifluoromethylphenyl)-4-methyl-5-*n*-propyl-1*H*-1,2,3-triazole (5). Yield 30%, mp 113.5–114.4 °C. ¹H NMR ($CDCl_3$) δ 0.88 (3H, t, J = 7.5 Hz,

(CH₂)₂CH₃), 1.46 (2H, sex, *J* = 7.5 Hz, CH₂CH₂CH₃), 2.41 (3H, s, CH₃), 2.46 (2H, t, *J* = 7.5 Hz, CH₂CH₂CH₃), 7.78 (2H, s, Ph). EIMS *m/z* (%) 27 (100), 281 (47), 283 (32), 337 (M, 10), 339 (M+2, 6.6). Anal. Calcd for C₁₃H₁₂Cl₂F₃N₃: C, 46.17; H, 3.58; N, 12.43%. Found: C, 46.24; H, 3.56; N, 12.51%.

3.1.8. 1-(2,6-Dibromo-4-trifluoromethylphenyl)-5-methyl-4-*n*-propyl-1*H*-1,2,3-triazole (6). Yield 14%, oily liquid. ¹H NMR (CDCl₃) δ 0.97 (3H, t, *J* = 7.4 Hz, (CH₂)₂CH₃), 1.80 (2H, sex, *J* = 7.4 Hz, CH₂CH₂CH₃), 2.10 (3H, s, CH₃), 2.72 (2H, t, *J* = 7.4 Hz, CH₂CH₂CH₃), 7.98 (2H, s, Ph). EIMS *m/z* (%) 43 (100), 368 (25), 370 (50), 372 (25), 425 (M, 2.4), 427 (M+2, 4.8), 429 (M+4, 2.4).

3.1.9. 1-(2,6-Dibromo-4-trifluoromethylphenyl)-4-methyl-5-*n*-propyl-1*H*-1,2,3-triazole (7). Yield 9%, 104.4–105.9 °C. ¹H NMR (CDCl₃) δ 0.83 (3H, t, *J* = 7.5 Hz, (CH₂)₂CH₃), 1.42 (2H, sex, *J* = 7.5 Hz, CH₂CH₂CH₃), 2.34 (3H, s, CH₃), 2.40 (2H, t, *J* = 7.5 Hz, CH₂CH₂CH₃), 7.91 (2H, s, Ph). EIMS *m/z* (%) 32 (100), 368 (48), 370 (96), 372 (48), 425 (M, 1.8), 427 (M+2, 3.6), 429 (M+4, 1.8).

3.1.10. 5-Methyl-4-*n*-propyl-1-(4-trifluoromethylphenyl)-1*H*-1,2,3-triazole (8). Yield 45%, mp 50.4–51.7 °C. ¹H NMR (CDCl₃) δ 1.01 (3H, t, *J* = 7.5 Hz, (CH₂)₂CH₃), 1.77 (2H, sex, *J* = 7.5 Hz, CH₂CH₂CH₃), 2.32 (3H, s, CH₃), 2.69 (2H, t, *J* = 7.5 Hz, CH₂CH₂CH₃), 7.64 (2H, d, *J* = 8.4 Hz, Ph), 7.82 (2H, d, *J* = 8.4 Hz, Ph). EIMS *m/z* (%) 212 (100), 226 (44), 241 (18), 269 (M, 5). Anal. Calcd for C₁₃H₁₄F₃N₃: C, 57.99; H, 5.24; N, 15.61%. Found: C, 57.91; H, 5.24; N, 15.28%.

3.1.11. 4-Methyl-5-*n*-propyl-1-(4-trifluoromethylphenyl)-1*H*-1,2,3-triazole (9). Yield 36%, oily liquid. ¹H NMR (CDCl₃) δ 0.79 (3H, t, *J* = 7.5 Hz, (CH₂)₂CH₃), 1.40 (2H, sex, *J* = 7.5 Hz, CH₂CH₂CH₃), 2.31 (3H, s, CH₃), 2.59 (2H, t, *J* = 7.5 Hz, CH₂CH₂CH₃), 7.52 (2H, d, *J* = 8.4 Hz, Ph), 7.74 (2H, d, *J* = 8.4 Hz, Ph). EIMS *m/z* (%) 212 (100), 226 (15), 241 (12), 269 (M, 6). Anal. Calcd for C₁₃H₁₄F₃N₃: C, 57.99; H, 5.24; N, 15.61%. Found: C, 57.92; H, 5.26; N, 15.36%.

3.1.12. 1-(2,6-Dichloro-4-trifluoromethylphenyl)-5-ethyl-4-*n*-propyl-1*H*-1,2,3-triazole (10). Yield 49%, oily liquid. ¹H NMR (CDCl₃) δ 1.00 (3H, t, *J* = 7.5 Hz, CH₂CH₃), 1.06 (3H, t, *J* = 7.5 Hz, (CH₂)₂CH₃), 1.82 (2H, sex, *J* = 7.5 Hz, CH₂CH₂CH₃), 2.53 (2H, q, *J* = 7.5 Hz, CH₂CH₃), 2.73 (2H, t, *J* = 7.5 Hz, CH₂CH₂CH₃), 7.78 (2H, s, Ph). EIMS *m/z* (%) 240 (36), 242 (25), 294 (100), 296 (65), 351 (M, 3), 353 (M+2, 2). Anal. Calcd for C₁₄H₁₄Cl₂F₃N₃: C, 47.75; H, 4.01; N, 11.93%. Found: C, 48.11; H, 4.08; N, 11.45%.

3.1.13. 1-(2,6-Dichloro-4-trifluoromethylphenyl)-4-ethyl-5-*n*-propyl-1*H*-1,2,3-triazole (11). Yield 33%, oily liquid. ¹H NMR (CDCl₃) δ 0.80 (3H, t, *J* = 7.6 Hz, (CH₂)₂CH₃), 1.29–1.41 (5H, m, CH₂CH₃ and CH₂CH₂CH₃), 2.40 (2H, t, *J* = 7.6 Hz, CH₂CH₂CH₃), 2.71 (2H, q, *J* = 7.6 Hz, CH₂CH₃), 7.71 (2H, s, Ph). EIMS *m/z* (%) 240 (39), 242 (27), 294 (100), 296 (66), 351 (M, 3), 353 (M+2, 2). Anal.

Calcd for C₁₄H₁₄Cl₂F₃N₃: C, 47.75; H, 4.01; N, 11.93%. Found: C, 47.88; H, 4.06; N, 11.75%.

3.1.14. 1-(2,6-Dichloro-4-trifluoromethylphenyl)-4,5-di-*n*-propyl-1*H*-1,2,3-triazole (12). Yield 33%, mp 69.8–70.9 °C. ¹H NMR (CDCl₃) δ 0.87 (3H, t, *J* = 7.5 Hz, (CH₂)₂CH₃-5), 1.00 (3H, t, *J* = 7.5 Hz, (CH₂)₂CH₃-4), 1.42 (2H, sex, *J* = 7.5 Hz, CH₂CH₂CH₃-5), 1.82 (2H, sex, *J* = 7.5 Hz, CH₂CH₂CH₃-4), 2.47 (2H, t, *J* = 7.5 Hz, CH₂CH₂CH₃-5), 2.72 (2H, t, *J* = 7.5 Hz, CH₂CH₂CH₃-4), 7.78 (2H, s, Ph). EIMS *m/z* (%) 308 (100), 310 (66), 365 (M, 3), 367 (M+2, 2). Anal. Calcd for C₁₅H₁₆Cl₂F₃N₃: C, 49.20; H, 4.40; N, 11.47%. Found: C, 48.97; H, 4.42; N, 11.17%.

3.1.15. 1-(2,6-Dichloro-4-trifluoromethylphenyl)-5-hydroxy-methyl-4-*n*-propyl-1*H*-1,2,3-triazole (13). Yield 26%, 87.3–87.7 °C. ¹H NMR (CDCl₃) δ 0.97 (3H, t, *J* = 7.4 Hz, (CH₂)₂CH₃), 1.79 (2H, sex, *J* = 7.4 Hz, CH₂CH₂CH₃), 2.16 (1H, s, CH₂OH), 2.76 (2H, t, *J* = 7.4 Hz, CH₂CH₂CH₃), 4.60 (2H, s, CH₂OH), 7.77 (2H, s, Ph). EIMS *m/z* (%) 296 (100), 298 (68), 353 (M, 1.1), 355 (M+2, 0.7). Anal. Calcd for C₁₃H₁₂Cl₂F₃N₃O: C, 44.09; H, 3.42; N, 11.86%. Found: C, 44.53; H, 3.53; N, 11.44%.

3.1.16. 1-(2,6-Dichloro-4-trifluoromethylphenyl)-4-hydroxy-methyl-5-*n*-propyl-1*H*-1,2,3-triazole (14). Yield 28%, 120.5–121.0 °C. ¹H NMR (CDCl₃) δ 0.89 (3H, t, *J* = 7.5 Hz, (CH₂)₂CH₃), 1.50 (2H, sex, *J* = 7.5 Hz, CH₂CH₂CH₃), 2.17 (1H, s, CH₂OH), 2.56 (2H, t, *J* = 7.5 Hz, CH₂CH₂CH₃), 4.86 (2H, s, CH₂OH), 7.81 (2H, s, Ph). EIMS *m/z* (%) 43 (100), 296 (12), 298 (8), 353 (M, 0.5), 355 (M+2, 0.3). Anal. Calcd for C₁₃H₁₂Cl₂F₃N₃O: C, 44.09; H, 3.42; N, 11.86%. Found: C, 44.17; H, 3.37; N, 11.82%.

3.1.17. 5-Chloromethyl-1-(2,6-dichloro-4-trifluoromethylphenyl)-4-*n*-propyl-1*H*-1,2,3-triazole (15) (Scheme 1). A mixture of **13** (128 mg, 0.36 mmol), thionyl chloride (1.6 g, 1 mL), and DMF (0.5 mL) was stirred at 85 °C for 30 min. The reaction mixture was concentrated and subjected to silica gel column chromatography (*n*-hexane/EtOAc = 20:1) to give **15** (90 mg, 0.24 mmol) as a yellowish solid. Yield 70%, 53.9–54.5 °C. ¹H NMR (CDCl₃) δ 1.01 (3H, t, *J* = 7.4 Hz, (CH₂)₂CH₃), 1.85 (2H, sex, *J* = 7.4 Hz, CH₂CH₂CH₃), 2.81 (2H, t, *J* = 7.4 Hz, CH₂CH₂CH₃), 4.45 (2H, s, CH₂Cl), 7.81 (2H, s, Ph). EIMS *m/z* (%) 240 (54), 242 (34), 294 (100), 306 (90), 308 (56), 371 (M, 2.1), 373 (M+2, 1.9), (M+4, 0.7). Anal. Calcd for C₁₃H₁₁Cl₃F₃N₃: C, 41.91; H, 2.98; N, 11.28%. Found: C, 41.66; H, 3.16; N, 10.86%.

3.1.18. 4-Chloromethyl-1-(2,6-dichloro-4-trifluoromethylphenyl)-5-*n*-propyl-1*H*-1,2,3-triazole (16). Compound **16** was synthesized by a method similar to that used for **15**. Yield 86%, 84.5–85.1 °C. ¹H NMR (CDCl₃) δ 0.92 (3H, t, *J* = 7.7 Hz, (CH₂)₂CH₃), 1.53 (2H, sex, *J* = 7.7 Hz, CH₂CH₂CH₃), 2.58 (2H, t, *J* = 7.7 Hz, CH₂CH₂CH₃), 4.80 (2H, s, CH₂Cl), 7.81 (2H, s, Ph). EIMS *m/z* (%) 240 (65), 242 (43), 306 (100), 308 (67), 371 (M, 7.2), 373 (M+2, 7), 375 (M+4, 2.4). Anal. Calcd

for C₁₃H₁₁Cl₃F₃N₃: C, 41.91; H, 2.98; N, 11.28%. Found: C, 41.84; H, 3.04; N, 11.08%.

3.2. Generation of *Drosophila* Schneider 2 (S2) cells stably expressing human $\beta 3$ GABA receptors

S2 cells expressing human $\beta 3$ GABA receptors were generated as previously described.¹⁹ Briefly, the cDNA encoding the $\beta 3$ subunit of the human GABA receptor (GenBank Accession No. NM_000814) was inserted into the *Drosophila* expression vector pMT (Invitrogen, Carlsbad, CA) to produce pMT-hs $\beta 3$, in which the expression of $\beta 3$ cDNA is driven by the metallothionein promoter and induced by copper sulfate. S2 cells were co-transfected with pMT-hs $\beta 3$ and the selection vector pCoHygro by a calcium phosphate transfection method, using a DES kit (Invitrogen) according to the manufacturer's instructions. The transfected cells were maintained for ~3 weeks in selection medium containing the antibiotic hygromycin B. Hygromycin B-resistant polyclonal cells were used for the binding assays as described in Section 3.5.

3.3. Construction of plasmid vectors containing human $\alpha 1$, $\beta 2$, and $\gamma 2$ GABA receptor subunits

Plasmid vectors, pCDM8-bovine(Bt)GABA_A $\alpha 1$ (NM_174540), which produces the amino acid sequence of the human $\alpha 1$ subunit, pCDM8-human(Hs)GABA_A $\beta 2$ (NM_000813), and pCDM8-human(Hs)GABA_A $\gamma 2$ (NM_000816), were obtained from the Neuroscience Research Center of Merck Sharp & Dohme Ltd (Harlow, Essex, UK). We changed the expression vector from pCDM8 to pcDNA3 (Invitrogen) for technical convenience. The 1.9 kb HindIII–XbaI BtGABA_A $\alpha 1$, the 1.5 kb XbaI–XbaI HsGABA_A $\beta 2$, and the 1.5 kb HindIII–HindIII HsGABA_A $\gamma 2$ fragments were inserted into the corresponding sites of pcDNA3 to produce pcDNA3 $\alpha 1$, pcDNA3 $\beta 2$, and pcDNA3 $\gamma 2$, respectively.

3.4. Stable expression of heteropentameric $\alpha 1\beta 2\gamma 2$ GABA receptors in HEK-293 cells

Human embryonic kidney-293 (HEK-293) cells were maintained in Dulbecco's modified Eagle's medium (DMEM; Gibco, Gaithersburg, MD) supplemented with 10% fetal bovine serum (FBS; Gibco) (complete DMEM) in a humidified incubator (5% CO₂ and 37 °C). For stable expression of proteins, the cells were transfected with vectors by the lipofection method and selected with the antibiotic G418 (Geneticin; Sigma–Aldrich, St. Louis, MO) according to the manufacturer's instructions. Briefly, aliquots of pcDNA3 $\alpha 1$ (0.5 μ g), pcDNA3 $\beta 2$ (0.5 μ g), and pcDNA3 $\gamma 2$ (5 μ g) were added to 100 μ L of OPTI-MEM I reduced serum medium (Gibco) and then mixed with 100 μ L of OPTI-MEM I medium containing 4 μ L of Lipofectamine (Invitrogen). The mixture was incubated at room temperature for 30 min, and then 0.8 mL of OPTI-MEM I medium was added. This solution was then overlaid onto 2×10^5 HEK 293 cells, which had been deprived of serum by washing with OPTI-MEM I medium, and incubated for 5 h. After the incubation, 1 mL of DMEM

containing 20% FBS was added to the dish. After a 24-h incubation, selection was started by replacing the old medium with complete DMEM containing G418 (1 mg/mL). After a ~2 week selection, resistant colonies were trypsinized in cloning cylinders and transferred to 24-well plastic plates. Individual monoclonal cell lines were expanded and cultured in the same medium.

The obtained cell lines were analyzed for the presence of subunit mRNAs by reverse transcription (RT) of total RNA followed by polymerase chain reaction (PCR). Total RNA was isolated from transfected HEK-293 cell lines using an Isogen kit (Nippon Gene, Toyama, Japan). RT was performed using an AMV reverse transcriptase kit (Life Sciences, St. Petersburg, FL) to synthesize cDNAs of $\alpha 1$, $\beta 2$, and $\gamma 2$ subunits. The RT products were then amplified by PCR using sets of primers annealing to the 5' and 3' ends of the genes. PCR products were checked by electrophoresis in 2% agarose gel. Cell lines that were positive for the presence of $\alpha 1$, $\beta 2$, and $\gamma 2$ transcripts were examined for their ability to specifically bind [³H]EBOB. Incorporation of $\gamma 2$ subunit into the ion channel was confirmed by [³H]diazepam binding assays as described by Hawkinson et al.⁴¹

3.5. Membrane preparation and [³H]EBOB binding assays

The membranes of S2 cells expressing $\beta 3$ receptors were prepared as previously described.¹⁹ Briefly, the S2 cells were grown in Schneider's *Drosophila* medium (Gibco) containing 10% FBS and hygromycin B (300 μ g/mL) in a shaking incubator (50 rpm) at 28 °C. S2 cells were grown at a viability of more than 96% and a density of $6\text{--}20 \times 10^6$ cells/mL of culture medium for 3–4 days. Copper sulfate was added to the medium at a concentration of 500 μ M/mL 24 h before the preparation of membranes. The S2 cells were homogenized in 10 mM Tris–HCl buffer containing 250 mM sucrose (pH 7.5) with a glass-Teflon homogenizer. The homogenate was centrifuged at 25,000g for 20 min. The resulting pellets were suspended in 10 mM sodium phosphate buffer containing 300 mM NaCl (pH 7.5) and used immediately for the binding assays.

The membranes of HEK-293 cells expressing $\alpha 1\beta 2\gamma 2$ receptors were prepared according to Yagle et al.⁴² The HEK-293 cells were cultured in complete DMEM and G418 (1 mg/mL) in 60-mm dishes to 100% confluent growth, and used for membrane preparation. The cells were harvested by scraping with 1 mL of a conditioned medium and centrifuged at 2000g for 10 min. The pelleted cells were suspended in 50 mM sodium phosphate buffer containing 200 mM NaCl (pH 7.4) and centrifuged at 2000g for 10 min. The washed cells were resuspended in the buffer and disrupted with a Polytron homogenizer (Kinematica, Lucerne, Switzerland). The homogenate was centrifuged at 25,000g for 30 min, and the resulting pellet was suspended in the buffer and used immediately for the binding assays.

[³H]EBOB binding assays were carried out as previously described.¹⁹ Briefly, S2 cell membranes (50 µg protein) expressing β3 receptors were incubated with various concentrations of phenyltriazoles and 0.5 nM [³H]EBOB in 1 mL of 10 mM sodium phosphate buffer containing 300 mM NaCl (pH 7.5) at 22 °C for 70 min. HEK-293 cell membranes (150 µg protein) expressing α1β2γ2 receptors were incubated with varying concentrations of phenyltriazoles and 1 nM [³H]EBOB in 1 mL of 50 mM sodium phosphate buffer containing 200 mM NaCl (pH 7.4) at 25 °C for 90 min. The protein content was determined by the method of Bradford.⁴³ After the incubation, the mixture was filtered through Whatman GF/B filters and rapidly rinsed twice with 5 mL of the incubation buffer (10 °C) using a cell harvester (M-24; Brandel, Gaithersburg, MD). The radioactivity of membrane-bound [³H]EBOB was measured with a liquid scintillation counter. Non-specific binding was determined in the presence of 5 µM unlabeled EBOB. Experiments were repeated at least three times. The IC₅₀ values were estimated from the mean values using the standard probit method. The K_i values were calculated using the Cheng–Prusoff equation $K_i = IC_{50}/(1 + [\text{radioligand}]/K_d)$.²¹ The K_d (apparent dissociation constant) values of EBOB for β3 (5.0 nM) and α1β2γ2 (10.7 nM) receptors were separately determined by Scatchard analysis.

3.6. Molecular modeling, CoMFA, and CoMSIA 3D-QSAR studies

The structures of all phenyltriazoles were constructed based on the X-ray crystal data of **21**¹⁹ using the CRY-SIN module in the molecular modeling software SYBYL ver. 7.1 (Tripos, St. Louis, MO) and were fully optimized by the semi-empirical molecular orbital method AM1. All the molecules were superposed at the 4-position of the phenyl group and the 1- and 4-positions of the triazole ring using the Fit Atoms menu of SYBYL. A conventional CoMFA was performed to study the 3D-QSAR of phenyltriazoles in β3 receptors using steric and electrostatic fields in SYBYL. All CoMFA calculations were performed with the SYBYL standard setup, that is, steric and electrostatic fields described by Lennard-Jones and Coulomb potentials, respectively, dielectric constant 1/*r*, and cutoff 30 kcal mol⁻¹ using an sp³ carbon atom with a charge of +1 as a probe atom.

CoMSIA was performed using the QSAR module in SYBYL. Steric, electrostatic, and hydrophobic contributions were evaluated using a common probe atom as used in CoMFA. The steric contribution was calculated using the third power of the atomic radii. The electrostatic field was determined by the application of semi-empirical AM1 MOPAC charges, and the hydrophobic field was derived from atom-based parameters. The attenuation factor (α) was defined as 0.3 and used as a default value.

The CoMFA and CoMSIA field descriptors were used as independent variables, and pK_i values were used as dependent variables in the PLS analysis to derive 3D-QSAR models. The K_i values of 1-phenyl-1*H*-1,2,3-triazoles in Tables 1–3 were converted to pK_i (–log K_i) values. The

predictive value of the models was first evaluated by leave-one-out cross-validation. The cross-validated correlation coefficient (*q*²) was calculated using the equation $q^2 = 1 - [\sum(Y_{\text{pred}} - Y_{\text{obs}})^2 / \sum(Y_{\text{obs}} - Y_{\text{mean}})^2]$, where *Y*_{pred}, *Y*_{obs}, and *Y*_{mean} are the predicted, observed, and mean affinity (pK_i) values of molecules, respectively. $\sum(Y_{\text{pred}} - Y_{\text{obs}})^2$ is the predictive residual sum of squares (PRESS). The optimum number of components corresponds to the highest *q*² and the lowest PRESS values in the cross-validated PLS analysis. The final 3D-QSAR models were obtained from non-cross-validated calculations using the optimum number of components. The CoMFA and CoMSIA results were graphically represented by field contribution maps using the field type 'stdev * coeff'.

3.7. Homology modeling and docking

The transmembrane segments of human β3 and α1β2γ2 GABA receptors were modeled using the cryo-electron microscopy structure of the nicotinic acetylcholine receptor of *T. marmorata* obtained at 4 Å resolution (PDB entry 1OED).²⁷ The sequences of the α1, β2, β3, and γ2 subunits were obtained from the protein Data-bank database (Accession Nos. α1, NM_174540; β2, NM_000813; γ2, NM_000816; β3, NM_000814). The subunit correspondence between the nicotinic acetylcholine and GABA receptors was assigned based on functional homology (Fig. 5B).⁴⁴ The multiple sequence alignment was performed with the MOE 2006.08 program (Chemical Computing Group, Montreal, Canada) using the PAM250 substitution matrix, and the long loop between TM3 and TM4 was deleted because of the lack of structure data in the template. About 20 intermediary models were generated by MOE, and the raw model with the best packing quality was further refined until the root mean square gradient became 0.01, according to the molecular mechanics minimization protocol using the Merck molecular field force MMFF94x⁴⁵ in MOE. In the mean time, the validation tests of stereochemical quality were conducted using MOE. Only 3 residues from the constructed β3 model and 4 from the α1β2γ2 model fell outside of the acceptable regions of the Ramachandran plot (data not shown). All bond angles, bond lengths, and Cα chiralities were also found to be adequate. The structures of 1-phenyl-1*H*-1,2,3-triazoles were built as described above. All the compounds were automatically docked into the potential binding site of β3 and α1β2γ2 receptors separately using the dock program in MOE. Each antagonist was subjected to conformational analysis, placement, and pharmacophore filtering, and was scored in terms of hydrophobic, ionic, and hydrogen-bond contacts, which were generally favorable interactions. A final docked representation of the potential binding mode of the ligands was chosen based on selection of the compound that possessed the best docking score within the most populated cluster with the lowest docking energy.

3.8. Insecticidal assays

The insecticidal activity of a representative disubstituted 1-phenyl-1*H*-1,2,3-triazole (**15**) was determined

following the previously described method.¹⁹ Briefly, different concentrations of **15** in acetone (1 μ L) were applied to the thoraces of adult female houseflies (WHO/SRS strain, 3–5 days after emergence) that were pre-treated with piperonyl butoxide (10 μ g in 1 μ L of acetone) 1 h before the application of **15**. Thirty houseflies were used for each dosage. The houseflies were maintained with sugar and water and were kept at 25 °C. The mortality rate was determined after 24 h, and the experiments were repeated three times. The LD₅₀ value was calculated from the mean mortality using the standard probit method.

Acknowledgments

We thank Merck Sharp & Dohme Ltd for supplying the GABA_A receptor plasmids. Part of this work was conducted at the Department of Molecular and Functional Genomics, Center for Integrated Research in Science, Shimane University.

References and notes

- Waldvogel, H. J.; Billinton, A.; White, J. H.; Emson, P. C.; Faull, R. L. M. *J. Comp. Neurol.* **2004**, *470*, 339–356.
- Akabas, M. H. *Int. Rev. Neurobiol.* **2004**, *62*, 1–43.
- Rabow, L. E.; Russek, S. J.; Farb, D. H. *Synapse* **1995**, *21*, 189–274.
- Barnard, E. A.; Skolnick, P.; Olsen, R. W.; Möhler, H.; Sieghart, W.; Biggio, G.; Braestrup, C.; Bateson, A. N.; Langer, S. Z. *Pharmacol. Rev.* **1998**, *50*, 291–313.
- Bonnert, T. P.; McKernan, R. M.; Farrar, S.; Le Bourdellès, B.; Heavens, R. P.; Smith, D. W.; Hewson, L.; Rigby, M. R.; Sirinathsinghji, D. J. S.; Brown, N.; Wafford, K. A.; Whiting, P. J. *Proc. Natl. Acad. Sci. U.S.A.* **1999**, *96*, 9891–9896.
- McKernan, R. M.; Whiting, P. J. *Trends Neurosci.* **1996**, *19*, 139–143.
- Buckingham, S. D.; Sattelle, D. B. In *Comprehensive Molecular Insect Science*; Gilbert, L. I., Iatrou, K., Gill, S. S., Eds.; Elsevier Pergamon: Amsterdam, 2004; Vol. 5, pp 107–142.
- french-Constant, R. H.; Mortlock, D. P.; Shaffer, C. D.; MacIntyre, R. J.; Roush, R. T. *Proc. Natl. Acad. Sci. U.S.A.* **1991**, *88*, 7209–7213.
- french-Constant, R. H.; Steichen, J. C.; Rocheleau, T. A.; Aronstein, K.; Roush, R. T. *Proc. Natl. Acad. Sci. U.S.A.* **1993**, *90*, 1957–1961.
- Ozoe, Y.; Akamatsu, M. *Pest Manag. Sci.* **2001**, *57*, 923–931.
- Zhao, X.; Yeh, J. Z.; Salgado, V. L.; Narahashi, T. *J. Pharmacol. Exp. Ther.* **2004**, *310*, 192–201.
- Grolleau, F.; Sattelle, D. B. *Br. J. Pharmacol.* **2000**, *130*, 1833–1842.
- Zhao, X.; Salgado, V. L.; Yeh, J. Z.; Narahashi, T. *J. Pharmacol. Exp. Ther.* **2003**, *306*, 914–924.
- Cole, L. M.; Nicholson, R. A.; Casida, J. E. *Pestic. Biochem. Physiol.* **1993**, *46*, 47–54.
- Ratra, G. S.; Casida, J. E. *Toxicol. Lett.* **2001**, *122*, 215–222.
- Ratra, G. S.; Kamita, S. G.; Casida, J. E. *Toxicol. Appl. Pharmacol.* **2001**, *172*, 233–240.
- Sammelson, R. E.; Caboni, P.; Durkin, K. A.; Casida, J. E. *Bioorg. Med. Chem.* **2004**, *12*, 3345–3355.
- Ozoe, Y.; Yagi, K.; Nakamura, M.; Akamatsu, M.; Miyake, T.; Matsumura, F. *Pestic. Biochem. Physiol.* **2000**, *66*, 92–104.
- Alam, M. S.; Kajiki, R.; Hanatani, H.; Kong, X.; Ozoe, F.; Matsui, Y.; Matsumura, F.; Ozoe, Y. *J. Agric. Food Chem.* **2006**, *54*, 1361–1372.
- Sieghart, W.; Sperk, G. *Curr. Top. Med. Chem.* **2002**, *2*, 795–816.
- Cheng, Y.; Prusoff, W. H. *Biochem. Pharmacol.* **1973**, *22*, 3099–3108.
- Cramer, R. D., III; Patterson, D. E.; Bunce, J. D. *J. Am. Chem. Soc.* **1988**, *110*, 5959–5967.
- Klebe, G.; Abraham, U.; Mietzner, T. *J. Med. Chem.* **1994**, *37*, 4130–4146.
- Böhm, M.; Stürzebecher, J.; Klebe, G. *J. Med. Chem.* **1999**, *42*, 458–477.
- Labrie, P.; Maddaford, S. P.; Fortin, S.; Rakhit, S.; Kotra, L. P.; Caudreault, R. C. *J. Med. Chem.* **2006**, *49*, 7646–7660.
- Kulkarni, R. G.; Srivani, P.; Achaiah, G.; Sastry, G. N. *J. Comput. Aided Mol. Des.* **2007**, *21*, 155–166.
- Miyazawa, A.; Fujiyoshi, Y.; Unwin, N. *Nature* **2003**, *423*, 949–955.
- Salany, A.; Zezula, J.; Tretter, V.; Sieghart, W. *Mol. Pharmacol.* **1995**, *48*, 385–391.
- Xu, M.; Covey, D. F.; Akabas, M. H. *Biophys. J.* **1995**, *69*, 1858–1867.
- Gurley, D.; Amin, J.; Ross, P. C.; Weiss, D. S.; White, G. *Receptors Channels* **1995**, *3*, 13–20.
- Perret, P.; Sarda, X.; Wolff, M.; Wu, T.-T.; Bushey, D.; Goeldner, M. *J. Biol. Chem.* **1999**, *274*, 25350–25354.
- Bell-Horner, C. L.; Dibas, M.; Huang, R.-Q.; Drewe, J. A.; Dillon, G. H. *Mol. Brain Res.* **2000**, *76*, 47–55.
- Zorov, B. S.; Bregestovski, P. D. *Biophys. J.* **2000**, *78*, 1786–1803.
- Buhr, A.; Wagner, C.; Fucks, K.; Sieghart, W.; Sigel, E. *J. Biol. Chem.* **2001**, *276*, 7775–7781.
- Chen, L.; Durkin, K. A.; Casida, J. E. *Proc. Natl. Acad. Sci. U.S.A.* **2006**, *103*, 5185–5190.
- Ci, S.; Ren, T.; Su, Z. *J. Mol. Model.* **2007**, *13*, 457–464.
- Hisano, K.; Ozoe, F.; Huang, J.; Kong, X.; Ozoe, Y. *Invert. Neurosci.* **2007**, *7*, 39–46.
- Ozoe, Y.; Ishikawa, K.; Tomiyama, S.; Ozoe, F.; Kozaki, T.; Scott, J. G. In *Synthesis and Chemistry of Agrochemicals Series VIII*; Lyga, J. W.; Theodoritis, G., Eds.; American Chemical Society: Washington, DC, 2007; ACS Symposium Series 948, pp 39–50.
- Hainzl, D.; Casida, J. E. *Proc. Natl. Acad. Sci. U.S.A.* **1996**, *93*, 12764–12767.
- Caboni, P.; Sammelson, R. E.; Casida, J. E. *J. Agric. Food Chem.* **2003**, *51*, 7055–7061.
- Hawkinson, J. E.; Drewe, J. A.; Kimbrough, C. L.; Chen, J.-S.; Hogenkamp, D. J.; Lan, N. C.; Gee, K. W.; Shen, K.-Z.; Whittemore, E. R.; Woodward, R. M. *Mol. Pharmacol.* **1996**, *49*, 897–906.
- Yagle, M. A.; Martin, M. W.; de Fiebre, C. M.; de Fiebre, N. C.; Drewe, J. A.; Dillon, G. H. *Neurotoxicology* **2003**, *24*, 817–824.
- Bradford, M. M. *Anal. Biochem.* **1976**, *72*, 248–254.
- Campagna-Slater, V.; Weaver, D. F. *J. Mol. Graphics Modell.* **2007**, *25*, 721–730.
- Halgren, T. A. *J. Comput. Chem.* **1996**, *17*, 490–519.
- Miller, C. *Neuron* **1989**, *2*, 1195–1205.